Journal of the Meteorological Society of Japan, Vol. 90, No. 2, pp. 297–310, 2012
DOI:10.2151/jmsj.2012-209

Role of Mesoscale Convective Systems Developed around the Eastern Tibetan Plateau in the Eastward Expansion of an Upper Tropospheric High during the Monsoon Season

Shiori SUGIMOTO

Graduate School of Environmental Science, Hokkaido University, Sapporo, Japan

and

Kenichi UENO

Faculty of Life and Environmental Sciences, University of Tsukuba, Tsukuba, Japan

(Manuscript received 26 May 2011, in final form 5 January 2012)

Abstract

In this study, we revealed and discussed the role of mesoscale convective systems (MCSs) in the eastward expansion of an upper tropospheric high (UH, that is South Asian High or Tibetan High) with a timescale of a few days over the Asian monsoon region in the summers of 1999–2008. The MCSs was extracted using hourly satellite images. The distribution of mature MCSs was inhomogeneous in the Asian summer monsoon region. At three specific regions, i.e., around the eastern part of Tibetan Plateau (TP), over the Bay of Bengal, and in northern Vietnam, the percentage of MCSs larger than 1.2×10^5 km^2 to all mature MCSs counted in each area was higher and exceeded 25%. Focusing on these regions, the UH extension was examined around the day of large MCSs (LMCSs) formation using objective analysis data sets. Only the LMCSs of eastern TP areas contributed to a significant increase of the geopotential height at 200 hPa with a temperature increase in the mid-upper troposphere. At the same time, the zone of active cloud convection (ZACC) was formed along 30–35°N over central and east China. Cyclonic circulation was strengthened in the eastern part of TP by the LMCS formation and transported moist air north and northeastward toward the inland region, such as the northeastern part of the Sichuan Basin, in the lower troposphere. This moisture advection corresponded to the meandering of the ZACC. The ZACC was maintained until a few days after the LMCS formation, and was also a contributor of greater extension of UH to the east and eastward propagation of the positive anomaly area of soil moisture.

1. Introduction

During the monsoon season, the center position of the upper tropospheric high (UH) distributed around the Tibetan Plateau (TP), which is generally called "South Asian High" or "Tibetan High," oscillates east and west in a sub-monthly time scale (Krishnamurti et al. 1973; Tao and Ding 1981). The relationship between the eastward expansion of UH and the formation of precipitation systems in and around China are particularly interesting. According to the statistical analysis of Yatagai and Yasunari (1995), an increase (decrease) in the summer precipitation at the Taklamakan Desert corresponds to the UH intensification (weakening) around 30°N, 100°E. In a year of heavy precipitation at the middle and lower areas of the Yangtze River, active cloud convections are formed by low-level convergence in association with anomalous moisture intrusion from the Bay of Bengal (BoB) and South China Sea due to enhancement of the Western Pacific Subtropical High over the northern South China Sea (Zhou and Yu 2005; Mao and Wu 2006). Under this condition, the active convections

Corresponding author: Shiori Sugimoto, Graduate School of Environmental Science, Hokkaido University, North 10 West 5, Kita-ku, Sapporo 060-0810, Japan
E-mail: shioris@ees.hokudai.ac.jp

strengthened the divergence in the upper troposphere and caused UH extension over China. Two different patterns of UH distribution, which are controlled by the variation of the propagation pathway of the Rossby wave along the subtropical jet, change the intraseasonal variability of cloud convective activity over the Yangtze River during Meiyu, as concluded through analysis of outgoing longwave radiation data from 1979 through 2004 (Fujinami and Yasunari 2009).

Active cloud convections during the Asian monsoon season contribute to the UH development via diabatic heating in the middle-upper troposphere. The latent heat release from convective clouds over and around the TP is known to be a factor for the maintenance of monsoon circulation and the first transition of the Asian summer monsoon (e.g., Nitta 1983; Yanai et al. 1992; Ueda and Yasunari 1998; Hsu et al. 1999). For the east-west oscillation of the UH, Zhang et al. (2002) reported that diabatic heating reached 200 hPa and was dominant in the case of the center position of UH staying over the TP, and adiabatic heating in the free atmosphere and diabatic heating near land surface were dominant in the case of the center position of UH staying over the Iran Plateau. On the other hand, Fujinami and Yasunari (2004) indicated that intraseasonal variability of cloud convection with sub-monthly time-scale oscillation over the southern TP is defined by the UH distribution, which is controlled by wave activity along the subtropical jet. During the pre-monsoon season, subsidence with adiabatic heating at the southwestern TP, which is a response of cloud activity in the tropical region, causes a high-pressure formation in the upper troposphere (He et al. 1987; Yanai et al. 1992; Tamura et al. 2010). According to a sensitivity experiment using five Atmospheric General Circulation Models (AGCMs) by Zhou et al. (2009), warming of the sea surface temperature and activation of cloud convection over the Indian Ocean–Western Pacific change the Walker circulation and weaken cloud activity over tropical central and eastern Pacific during the monsoon season. This response from ocean to atmosphere encourages westward extension of the eastern Pacific subtropical high in the middle troposphere and expansion of UH. Previous studies have focused on UH distribution with a time scale of 10 days to several months, and have used daily OLR/Tbb data, objective analysis/reanalysis data, and simulated results with grid spacing of a few hundred km. However, these data do not sufficiently represent the active diurnal variation of mesoscale organized clouds that are a dominant component of convection in Asian summer monsoons. A new index defined by hourly satellite images will assist in the understanding of the direct impact of active cloud convection on UH enhancement with "a timescale of a few days."

Mesoscale convective systems (MCSs) are cloud systems that are expected to heat the atmosphere efficiently in a time scale from several hours to 1–2 days. Since the 1980s, the generation of large cloud systems has been observed by satellites in the Asian monsoon region. For example, large cloud clusters with radii larger than 140 km and a lifetime of 10–50 hours tend to occur intensively in the northern part of the Bay of Bengal (BoB) and propagate south-southwestward (Zuidema 2003). Houze et al. (2007) has explained that an MCS at the foothill of the steep terrain of the Himalayas is formed by the enhancement of convective instability due to the intrusion of a moist monsoon flow over the dry air mass from the TP. Although the Himalayas and the TP are inland with high elevations and low humidity, MCS generation has been confirmed by Barros et al. (2004) and Li et al. (2008). According to a numerical simulation of Sugimoto and Ueno (2010), cyclonic circulation induced by land surface heating in the dry western TP and its eastward propagation during the nighttime induce a low-level convergence over the wet eastern TP on the following daytime, and this convergence is a trigger for large MCS generation. Case studies of the early 2008 monsoon season by Ueno et al. (2011) indicate that a large MCS is generated at the Sichuan Basin in the evening by strengthening of the low-level convergence between the southerly monsoon flow and northerly dry intrusion under conditions of a following mid-latitude trough. Xie and Ueno (2011) also clarifies that intensive generated areas of the MCSs in the Sicuan Basin overlap with areas recording heavy rains accompanying severe disasters. It would be valuable to examine the contribution of those MCSs to the 1–2 day variation of synoptic fields, including upper tropospheric pressure pattern in East Asia.

In our study, the impact of cloud activity on the eastward extension of UH was revealed within 1–2 days, focusing on an MCS with a meso-alpha scale. The analysis period is from June through August from 1999 to 2008 (10 years), and set at 64–124°E, 14.5–46.5°N. First, the MCSs were extracted and tracked in the target region using satellite hourly images. The distribution of MCSs and initiation/maturity time were identified. Next, the differences in the temperature/geopotential height were calculated between the day of MCS development and the day before MCS generation, and effective areas of MCS development on the UH intensification were examined. Finally, convective activity was analyzed around the effective area on the day of and a few days following MCS formation, and its function on

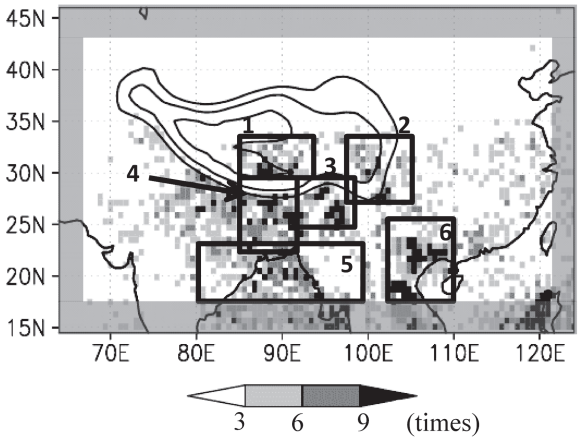

Fig. 1. Frequency distribution of mature MCS counted at every 0.6 degrees of grid spacing in the summer from 1999 to 2008. Elevations are contoured from 3000 to 5000 m at 1,000-m intervals. Six concentrated areas of the MCS development are marked by open squares, and Area 4 and Area 6 (Area 5) include only land (ocean) area. The gray zone is not included in the analysis.

further UH expansion and change in land-surface conditions were discussed.

2. Data description

Infrared (IR) images of Meteosat5 (until 2006) and Meteosat7 (from 2007) provided by EUMETSAT were used for the analysis of cloud convections. Meteosat5/7 is a stationary satellite located over the Indian Ocean at 63°E, 0°N/57°E, 0°N. The horizontal data resolution is about 5 km at the nadir, and an original image is composed by perspective projection with inhomogeneous grid spacing. The original data was transformed into brightness temperature (Tbb) with a conversion table. The Tbb of Meteosat7 was intercalibrated with that of Meteosat5 to adjust observation error. $0.3^\circ \times 0.3^\circ$ gridded data was produced because the original data with inhomogeneous grid spacing was inconvenient for the calculating the area and tracking of an MCS. The farthest grid point from the stationary position of the satellite, which is 124°E, 46.5°N, includes 2–5 original data for averaging to create gridded data.

The Japanese Meteorological Agency (JMA) conducted a Japanese 25-year ReAnalysis (JRA25) in collaboration with the Central Research Institute of Electric Power Industry (Onogi et al. 2007). The reanalysis period was from January 1979 to December 2004. The resolution of a global model for producing the JRA25 is T106L40 with a model top of 0.4 hPa. JMA also operates a real-time climatic assimilation system known as the JMA Climate Data Assimilation System (JCDAS) using the same system as JRA25. The JCDAS products have been available since January 2005. We used pressure-level analysis data of JRA25 (until 2004)/JCDAS (from 2005) with 1.25° grid-spacing in this study to analyze the fluctuation of the synoptic condition.

The soil moisture data from the Advanced Microwave Scanning Radiometer for Earth observing system (AMSR-E) estimated by Fujii et al. (2009) from 2003 to 2008 was also used to analyze the land surface condition. Fujii et al. revised the soil moisture algorithm of Koike et al. (2004) to increase the accuracy using a new fractional vegetation coverage dataset which was created from the normalized difference vegetation index (NDVI) provided as a standard product using the Moderate Resolution Imaging Spectroradiometer (MODIS). AMSR-E can be used to observe around the TP region approximately once a day. The data resolution is 1.25° grid spacing, and the number of significant figures for soil moisture is 0.001 (cm^3 cm^{-3}).

3. MCS tracking method

The MCS was extracted using IR images of Meteosat5/7. The methods of the MCS extraction and tracking conformed to those of Evans and Shemo (1996). Their methods have been applied to the region around the Himalayas and TP by Barros et al. (2004), Sugimoto and Ueno (2010), and Ueno et al. (2011). First, a continuous area larger than 4,000 km^2 and with Tbb less than 219 K (hereafter, the target cloud area) was identified. A Tbb threshold with 219 K is appropriate over the plateau because the echo top of convective precipitation observed by Doppler radar in the central TP, as pointed by Uyeda et al. (2001), reached 17 km above sea level. If grids with Tbb less than 235 K existed around the target cloud area, the grids were treated as candidate areas for MCS. This requirement allows the criteria of cumulus convections with precipitation. Next, target cloud areas at time t were compared with the image obtained one hour later $(t+1)$. If the overlapped areas of target cloud of time $= t$ and $t+1$ exceeded 40% or if this overlap was greater than 10^4 km^2, they were categorized as the same target cloud area. Target clouds tracked for more than 6 hours were determined as MCSs. If two target cloud areas merged, the larger one was chosen for continued tracking. The smaller one was not ignored if its lifetime was longer than 6 h; however, active tracking was terminated. In

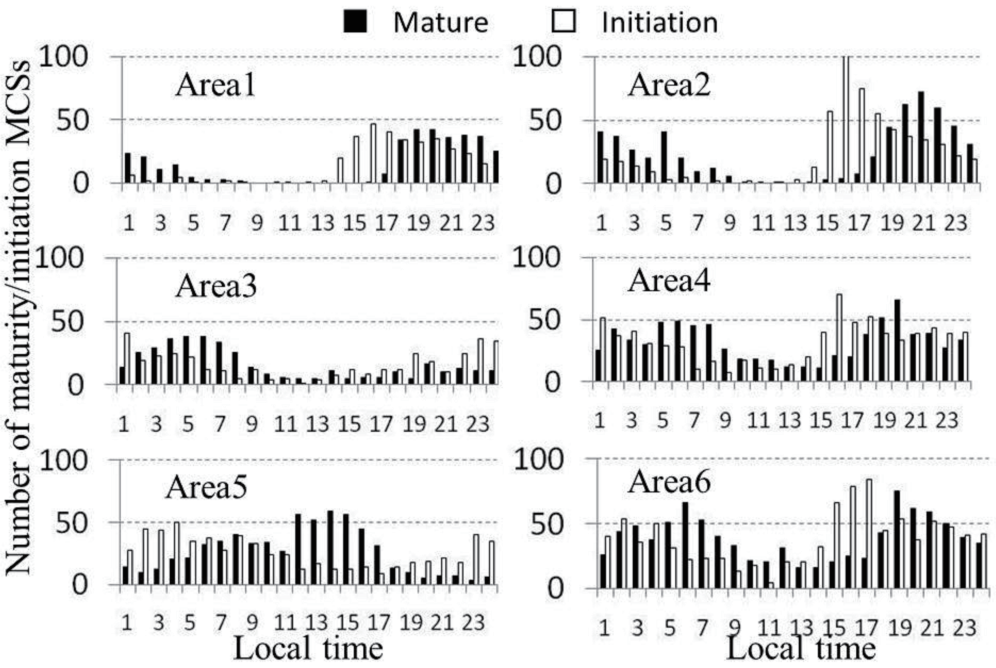

Fig. 2. Frequency distribution of the initiation (white) and mature (black) time of the MCS in each area. The horizontal axis shows the local time depending on each longitude.

this study, a grid with a minimum Tbb was identified as the location of MCS and tracked to calculate the MCS movement. Missing images of less than 3 hours were interpolated on a time sequence and MCS tracking was continued. "Mature size/mature time" was defined as the size/time when each tracking MCS reached the maximal area. Tracking results including areas three degrees to the left, right, top and bottom of the analysis area were not used because the MCS generated in edge had possibility to go outside of the analysis area before the MCS extinction.

4. MCS formation around the TP

A ten-year location composition with mature size MCSs is shown in Fig. 1. The MCSs developed in several concentrated areas; some of them were over ocean and coastal areas, and others were over inland and high elevation areas. The generation and growth of cloud convective systems in the former areas have been explained by solar radiative heating during daytime (e.g., Chen and Houze 1997) and low-level convergence between prevailing flow and local circulation, such as land/mountain breeze during the nighttime (e.g., Ohsawa et al. 2001; Zuidema 2003). On the other hand, MCS development in high and inland areas, such as the latter, was interesting because these areas were supposed to have scarce water vapor. In our study, six areas were selectively defined: 1) southern TP, 2) eastern TP and western edge of the Sichuan Basin, 3) Patkai Mountains, 4) southern Himalaya lowlands, 5) Bay of Bengal (BoB), and 6) northern Vietnam and southern coastal area of China (labeled in Fig. 1), and the growth rate of large MCS was investigated for each of the six areas. The number of MCSs/very large MCSs exceeding 1.2×10^5 km^2 (about the top 20% of all MCSs in the Asian monsoon region) was 1) 344/76, 2) 564/141, 3) 380/22, 4) 765/165, 5) 628/321, and 6) 933/276, respectively. The incidence rate of very large MCSs to all mature MCS counted in each area exceeded 25% in three areas, i.e. Areas 5 (51.1%), 6 (29.6%) and 2 (25.0%). It is especially notable that one MCS was formed per day on average in Area 6 and one-half of the MCSs over the BoB (Area 5) grew larger than 1.2×10^5 km^2. This means that MCSs were frequently generated and developed over those ocean and coastal areas. It is also noteworthy that very large MCSs easily developed around the eastern part of TP (Area 2) relative to other high elevation (Area 1) and inland areas (Area 3).

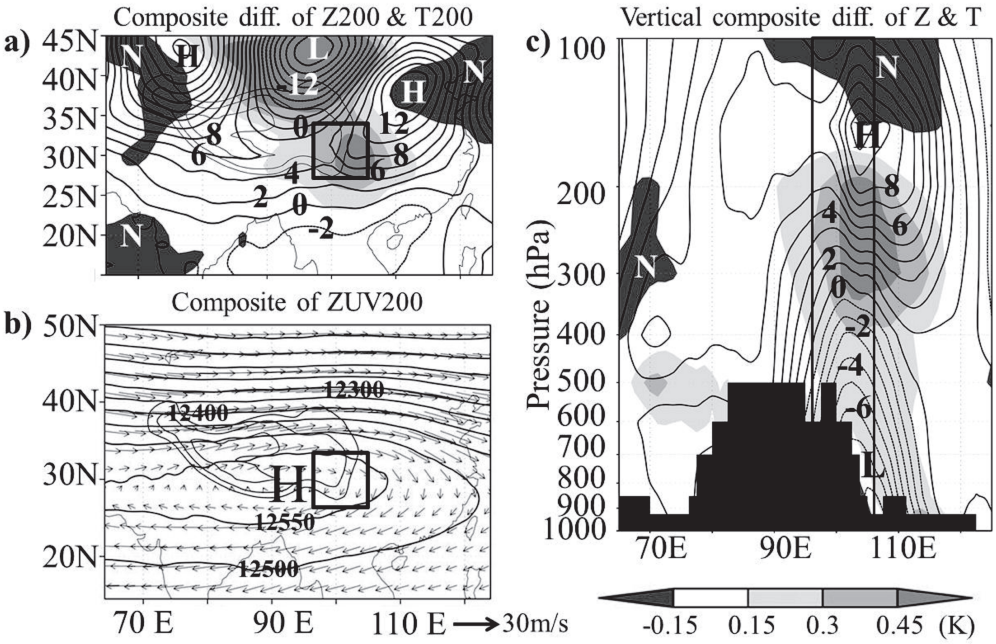

Fig. 3. a) Composite diff. of the temperature (shaded, K) and geopotential height (contour, gpm) at 200 hPa, b) composite distribution of the wind (vector, m s^{-1}) and geopotential height (contour, gpm) at 200 hPa, and c) longitude-vertical cross section of the composite diff. of temperature (shaded, K) and geopotential height (contour, gpm) along 30°N in the LMCS cases of Area 2. The scale of shades in Fig. 3a is the same as that in Fig. 3c. "L," "H," and "N" indicate "a low geopotential height anomaly", "a high geopotential height or its anomaly," and "a negative value of temperature anomaly," respectively. The topography is masked out with black in Fig. 3c.

Diurnal variation of initiation and mature time of MCSs was examined in six areas, as shown in Fig. 2. First, over the TP (Areas 1 and 2), the primary time of MCS occurrence was 15–17 local time (LT), which corresponds with the result of Li et al. (2008). MCSs reached maturity at 19–23 LT and there was a blank in MCS formation at 9–13 LT. Only in Area 2, the diurnal variation of cloud activities was the most significant for all target areas, and mature time had another small peak at 01–02 LT. According to rain data obtained by gauge observation and satellite estimation in the eastern periphery of TP, the hourly precipitation amount and precipitation intensity reached their maximum at night over high land area and midnight in the low land area (Yu et al. 2007; Zhou et al. 2008). The two peak maturity times in Area 2 conformed to precipitation observations shown in the previous studies.

The major timing of MCS initiation (maturity) in Area 3 was 22–01 LT (4–7 LT), this area was consistent with the midnight precipitation area shown in Ohsawa et al. (2001). The frequency distributions of MCS formation in Areas 4 and 6 were characterized by double peaks. The MCSs tended to form in the afternoon or midnight, and reached maturity after 2–4 hours of generation in each area. The double peaks in MCS initiation/maturity corresponded to the diurnal variation of cloud activity and the amount of precipitation shown in Islam et al. (2004) using IR satellite data and Ohsawa et al. (2001) with rain gage observation. Finally, the active convective time over the ocean area (Area 5) differed substantially from that in the continental areas. The MCS initiation times concentrated from 23–04 LT, and maturity time had two maximum peaks; the smaller one was around 08 LT, and the larger one was around 12–15 LT. The smaller morning peak of maturity time of MCSs corresponded to the diurnal variation of convective cloud activity formed over the BoB shown in Yang and Slingo (2001). On the other hand, Zuidema (2003) indicated the midnight–early morning initiation of cloud clusters (with radii larger than 210 km and Tbb lower than 210 K) and maturity from morning through noon over the BoB. Islam et al. (2004) also showed that

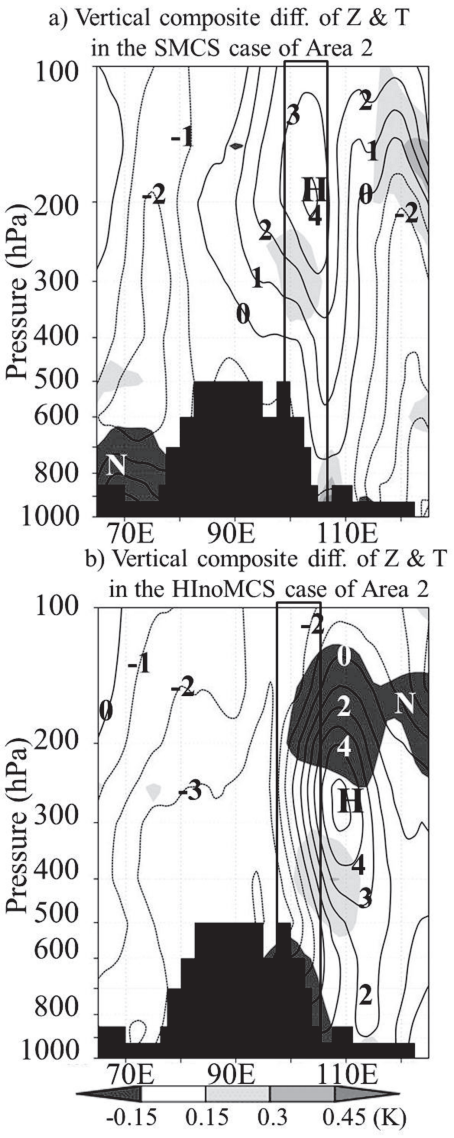

Fig. 4. Same as Fig. 3c, but for the a) SMCS case and b) HInoMCS case of Area 2.

cloud embedded area with Tbb lower than 214 K maximized in the afternoon over the northern part of the BoB. The initiation timing and larger peak in maturity times of the MCSs in Area 5 of our study was consistent with their results.

According to MCS tracking, the maturity size/time of the MCS clearly differed from region to region in the Asian monsoon area, and significant incidences of very large MCSs were recognized in not only the ocean and coastal areas (Areas 5 and 6) but also inland high elevation area (Area 2). MCS formation with obvious diurnal variation around the eastern TP is expected to play a direct role in day-to-day variability of UH. The impact of large MCSs on the UH enhancement was investigated focusing on Areas 2, 5, and 6, as shown in the next section.

5. Identifying an area with significant variation of synoptic conditions associated with MCS formation

The convective index (Ic), which is defined as either Ic = "threshold temperature" − Tbb (when Tbb is not exceeding a threshold) or Ic = 0 (otherwise), has been used for the analysis of cloud convective activity for ease of calculation (e.g., Murakami 1983; Fujinami and Yasunari 2001, 2004). However, the Ic cannot directly represent the size of convective cloud systems and lifetime of a convective cloud. Three categories were then developed for this study: 1) a case of MCS development to large size (LMCS), 2) a case of MCS formation without further growth (SMCS), and 3) a case of high daily averaged Ic without MCS formation (HInoMCS). For each target area, the days in the top or bottom 15% during a mature MCS were extracted for LMCS or SMCS cases. On a no-MCS formation day, if the daily-mean Ic was larger than the climatological Ic averaged during Jun.–Aug. in 1999–2008, that day was classified as a HInoMCS case. The threshold temperature of this study was set at 250 K for the calculation of Ic. The number of LMCS/SMCS/HInoMCS cases was 86/85/110 for Area 2, 199/202/28 for Area 5, and 193/199/70 for Area 6, respectively. For the temperature and geopotential height, the composite of the difference between the selected days for each case and a day before the target MCS generation (a day before the selected day) was calculated for the LMCS and SMCS (HInoMCS) cases to examine the influence of MCS on the UH fluctuation using JRA25/JCDAS. Hereafter, the abbreviation "composite diff." is used for convenience.

First, the impact of LMCSs that developed in Area 2 on the synoptic condition in the upper troposphere was investigated. The composite diff. of geopotential height and temperature at 200 hPa for the LMCS case of Area 2 is shown in Fig. 3a. A high-low-high anomaly pattern appeared alternately on the geopotential pattern with 15–20 degree intervals to the north of 38°N where the sub-tropical jet dominated (Fig. 3b). The train of high/low anomalies with cold/warm temperature anomalies had a wave number of 8 (not shown). Terao (1998) revealed that a quasi-stationary Rossby wave with a 5–7 wave number, which has an approximate 14-day or 30–45-day time scale, is formed along

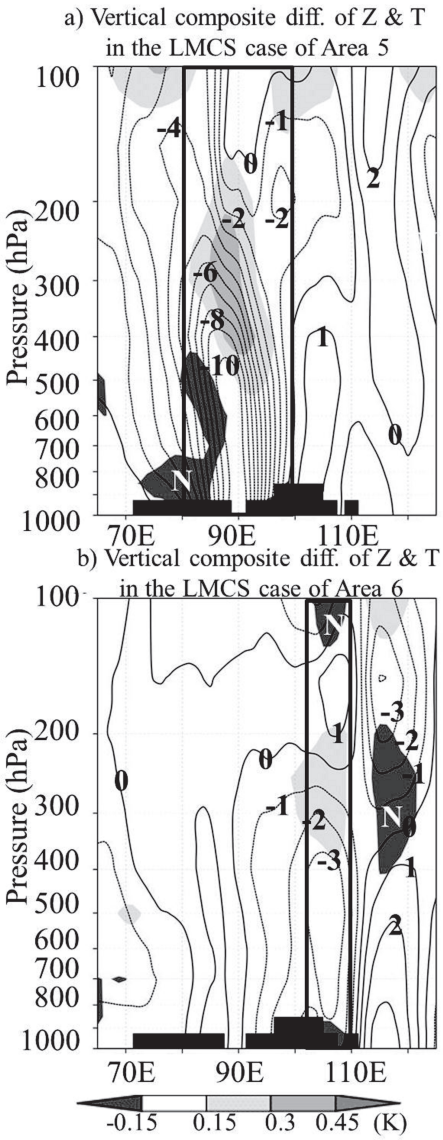

Fig. 5. Same as Fig. 3c, but for the LMCS cases of a) Area 5 and b) Area 6 along 20°N.

the sub-tropical jet during summer in the northern hemisphere. Eastward propagation of the quasi-stationary Rossby wave with a sub-monthly scale contributes to the formation of the Bonin high (Enomoto et al. 2003) and controls the intraseasonal variability of cloud convections over the southern TP (Fujinami and Yasunari 2004). The high and low anomalies of geopotential height shown in Fig. 3a were a part of the mid-latitude wave activity. On the other hand, no significant wave propagation was found in the mid-latitude for the composite cases of SMCS and HInoMCS (not shown). This result indicated that the mid-latitude wave activity contributed to the MCS "growth" in Area 2.

The local temperature around 30°N, 105°E increased more than 0.45 K at the time between initiation and maturity of an LMCS (shade pattern in Fig. 3a), and the center of temperature increase slightly shifted to the southeast due to a northerly-northwesterly at 200 hPa, as shown in Fig. 3b. In addition, a high pressure anomaly in a geopotential height field with a center located at 40°N, 110°E extended southwestward because of the response to the local temperature increase associated with MCS formation. According to the vertical structure of the composite diff. along 30°N (Fig. 3c), the temperature increased between 400 and 200 hPa level, and a high anomaly of geopotential height with 8–10 gpm appeared between 200 and 100 hPa. For the SMCS (HInoMCS) case, a weak temperature increase of 0.15–0.3 K was recognized at 350–250 (500–300) hPa (Figs. 4a and 4b). The geopotential height in the upper troposphere of the SMCS case increased only 4 gpm, which is less than half of the magnitude of the LMCS case. There was no variation of the geopotential height at 200 hPa on the longitude of Area 2 in the case of HInoMCS. Consequently, only large cloud systems could contribute greatly to the 1–2-day strengthening of the UH and temperature increase in Area 2.

Next, the synoptic circulation variation was examined in the case of LMCS formation over Areas 5 and 6. For the LMCS cases of Area 5, a longitude-vertical cross section along 20°N of the composite diff. showed 6–10 gpm decrease of the geopotential height from the surface to 300 hPa and 0.3–0.45 K temperature increase at 450–200 hPa within 1–2 days corresponding to the LMCS development (Fig. 5a). A weak temperature increase in a 400–200 hPa layer with small positive anomaly in geopotential height for 200–150 hPa was also identified in LMCSs cases of Area 6 (Fig. 5b). The increases in temperature and geopotential height ranges for the LMCS cases in both areas were small relative to those in Area 2. According to a synoptic chart at 850 and 500 hPa for the LMCS cases of Areas 5 and 6 (not shown), an obvious cyclonic circulation was formed in each area. Zuidema (2003) has pointed out that a large organized cloud system with Tbb below 210 K was formed with development of a cyclone and monsoon depression over the northwestern BoB. According to the analysis using geostationary meteorological satellite images at the Indian monsoon region by Laing and Fritsch (1993), some mesoscale convective complexes develop into tropical depressions. The tropical cyclones that form over the South China Sea and east of

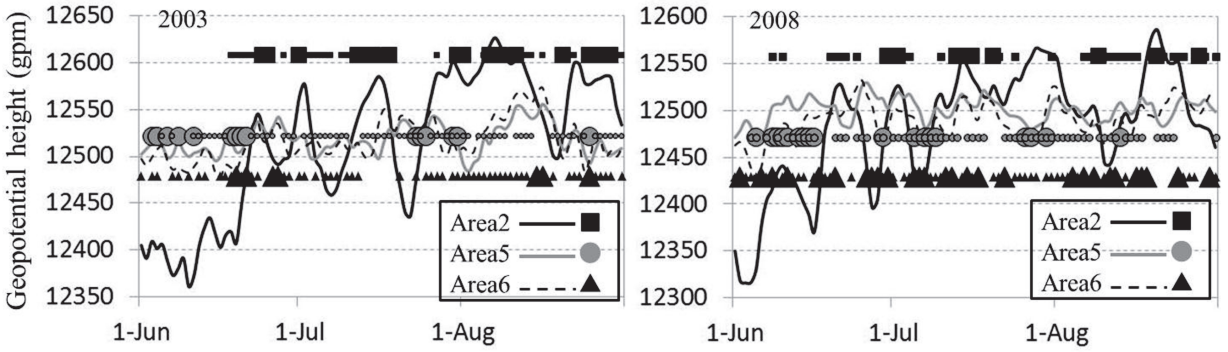

Fig. 6. Daily mean of geopotential height in 2003/2008 summers averaged in Areas 2 (black thick line), 5 (gray line), and 6 (black dashed line). Large (small) squares, circles, and triangles mean LMCS (MCS excluding LMCS) formation days in Areas 2, 5, and 6, respectively.

the Philippines, which accounted for 33% of all tropical cyclones, pass over the coastal region of South China and northern Vietnam and cause landfall due to heavy rainfall (Camargo et al. 2007). The development of such disturbances over the BoB and the northern part of Vietnam, as shown in previous studies, was expected to form LMCS and caused a rapid decrease of the geopotential height anomaly in the lower and middle troposphere with a weak temperature increase in the middle and upper troposphere. On the other hand, the temperature increase between the middle and upper troposphere was not captured in the SMCS and HInoMCS cases in Areas 5 and 6 (not shown).

On a monthly time scale, latent heating from active cloud convections, including MCSs in the sub-tropical areas such as Areas 5 and 6, play an important role in the first transition to Asian summer monsoon and maintenance of monsoon circulation (e.g., Li and Yanai 1996; Hsu et al. 1999). However, the upper tropospheric geopotential height increased significantly on a 1–2 day time scale only in the LMCS case in Area 2. We need to explore the reasons why the LMCS in Areas 5 and 6 did not show a large effect on the day-to-day fluctuation of UH directly above the subtropical region. Figure 6 shows the temporal sequence of the daily geopotential height averaged in Areas 2, 5, and 6 at 200 hPa during the summers of 2003/2008, which were active years of LMCS formation in Area 2/Areas 5 and 6, as examples. The amplitude and behavior of intra-seasonal variability in geopotential height were significantly different between Area 2 and Areas 5 and 6 for both years. In Area 2, geopotential height increased to about 150 gpm at the monsoon onset in mid-June. Then, a 10–20-day oscillation with large amplitude, which was about 100 gpm for a few days, was prominent. In most cases, the LMCS formation in Area 2 corresponded to the maximal phase of the geopotential height. For Areas 5 and 6, the fluctuation in the upper geopotential height was about one-third to one-half of that of Area 2 without a seasonal trend. The LMCS formed independently of the variation in geopotential height in the upper troposphere. Those relationships between geopotential height and LMCS formation in each area were also shown in other years (not shown). The temperature fluctuation at 200 hPa was 2–2.5 K in Areas 5 and 6 with a 10–20-day time scale, and about one-half of that in Area 2 (not shown). As described in Section 4 and shown in Fig. 6, the cloud convective systems, i.e. including not only the LMCS but also medium or small MCSs, formed in Areas 5 and 6 on consecutive days. We speculated that those active cloud convections reduced the geopotential height and temperature variations on a 1–2-day time scale around the center area of the UH.

LMCSs in Areas 5 and 6 could not drastically change the geopotential height in the upper troposphere, unlike the LMCS case of Area 2. Tamura et al. (2010) indicated that the remote response of cloud convection in the Southeast Asian/Indian monsoon region was a factor to make adiabatic subsidence over the southwestern TP during the pre-monsoon season. A remote response to UH expansion was also confirmed by composite analysis of the pressure vertical p velocity and geopotential height. The updraft was analyzed over the BoB and the northern part of the South China Sea in both LMCS cases of Areas 5 and 6, not only at 200 hPa as shown in Figs. 7a and 7b, but also between the surface and the

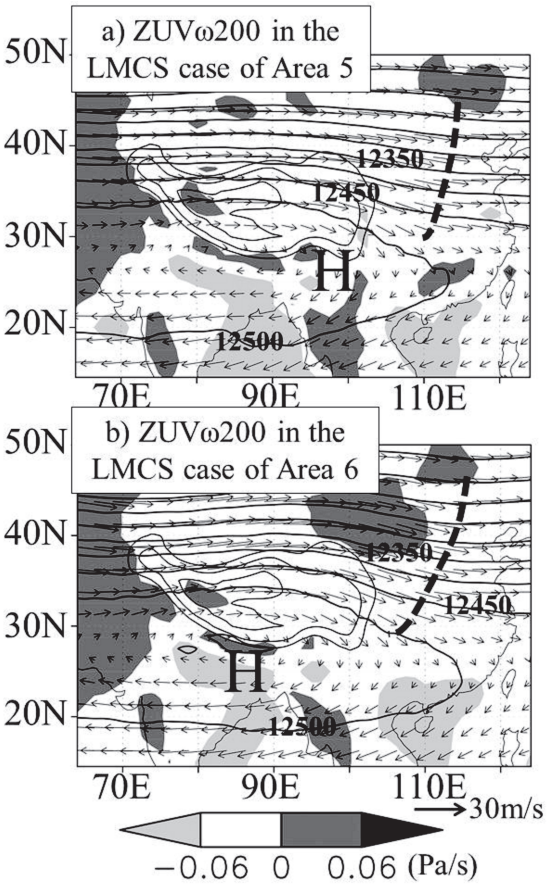

Fig. 7. Same as Fig. 3b, but for the LMCS cases of a) Area 5 and b) Area 6 with vertical p velocity (shaded; Pa s^{-1}). The dashed line indicates an axis of a synoptic trough.

upper troposphere. On the other hand, the weak downdraft appeared over the southwestern part of the Indian subcontinent, over the land east of the BoB, some areas north of 40°N, and over the continent west of 75°E. The weak subsidence areas shown in Fig. 7 did not correspond to the area of UH expansion, which is the focus of this study. In other words, we could not find any areas of subsidence over central and east China in LMCS cases in Areas 5 and 6. In addition, the synoptic scale midlatitude trough existed at 200 hPa over central and east China in LMCS cases for both Areas 5 and 6 (dashed line in Figs. 7a and 7b, respectively). The distribution of 12500-gpm isoline shifted slightly southward between 100 and 113°E, and its eastern edge remained at about 10 degrees west of that in the Area 2 LMCS case, as shown in Fig. 3b. This evidence does not indicate any impact of the remote response of convective activity in the sub-tropical region on UH expansion to the east on a 1–2 day time scale.

6. Formation of active cloud convection zone and its impact on the UH fluctuation after the LMCS development around the eastern TP

The LMCS around the eastern part of TP was a direct factor for the eastward extension of UH on a 1–2 day time scale. In this section, the variation of the UH, land surface condition, and cloud activity in the surrounding region of Area 2 were examined after LMCS development. The daily maximum value of Ic (Icmax) was defined as another index of cloud convection in addition to the MCS tracking, and the difference between the composite of the Icmax of LMCS cases and its climatology averaged during Jun.–Aug. 1999–2008 was calculated. Hereafter, the day of LMCS development is represented as $t = 0$, and the number of days before (after) is described as $t = -1, -2, -3, -4, -5$ ($t = +1, +2, +3, +4, +5$).

First, the contribution of the LMCS to the cloud convection over China was investigated on the day of LMCS development. An area with positive anomaly of Icmax larger than 4 K extended eastward to 93°E along 32°N on $t = 0$ (Fig. 8a) and was defined as a Zone of Active Cloud Convection (ZACC). The maximum center of the Icmax anomaly was located in Area 2 as a peak of ZACC. The formation of a very large MCS concentrated in Area 2 with an altitude higher than 1500 m (Fig. 8b). In the case of LMCS development, cyclonic circulation over Area 2 was stronger than that of the climatology and enhanced intrusion of moist southerlies at 700 hPa to the east of 105°E (Fig. 8a). The ZACC clearly curved inland in association with those enhanced moisture intrusions, although the northeastern side of the Sichuan Basin (around 110°E, 35°N) was without very large MCS formation. This evidence indicated that the LMCS around the eastern TP functioned as the northward-northeastward moisture transport and activated cloud convection inland.

Next, we analyzed the linkage among the UH eastward extension, land surface wetness, and the LMCS/ZACC activity after a few days of LMCS formation. The anomalies, which are the LMCS cases minus climatology, averaged 30–35°N; a) Icmax, b) geopotential height at 200 hPa, and c) daily soil moisture from $t = -5$ to $t = +5$ are shown in Fig. 9. Four days prior to LMCS formation ($t = -4$), cloud convections were activated over two zones; one was from 82 to 107°E, and the other was east of 115°E (Fig. 9a). The upper geopotential height gradually increased following the

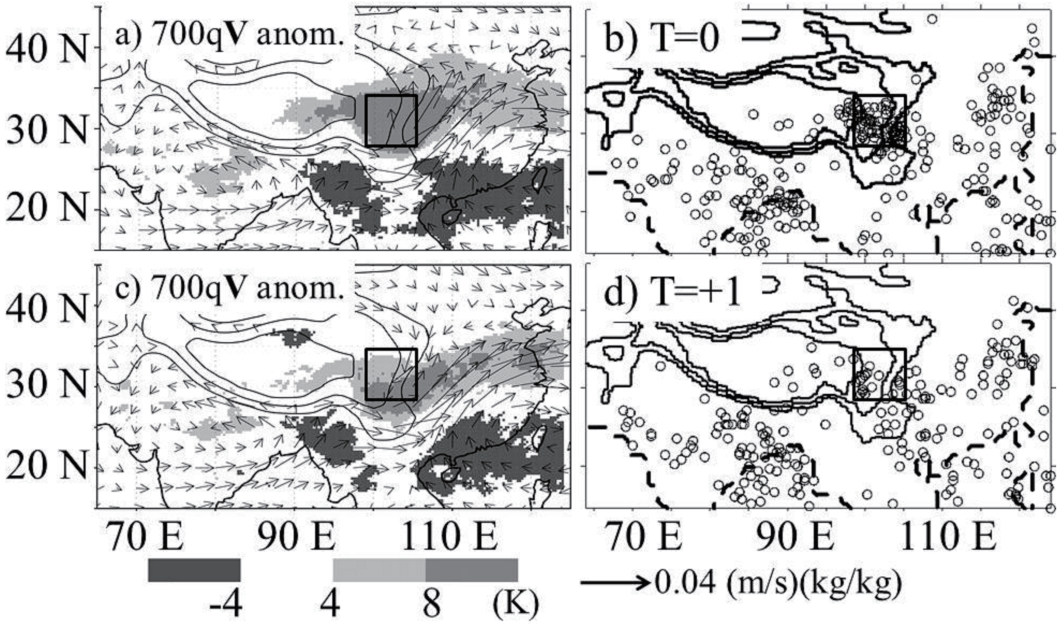

Fig. 8. (Left) Composite of Icmax (shaded) and $q\mathbf{V}$ (vector) anomaly from climatology a) on the day of LMCS formation in Area 2 ($t = 0$) and c) a day after LMCS formation ($t = +1$). A thin contour indicates topography with 1,500, 3,000, and 4,500 m above sea level of JRA25, and a thick line indicates the coastline. An open square shows Area 2. (Right) Distribution of the position of mature MCS larger than 1.2×10^5 km^2 b) on the day of LMCS formation in Area 2 ($t = 0$) and d) a day after LMCS formation ($t = +1$). A thick contour indicates topography with 1,500, 3,000, and 4,500 m above sea level, and a thick dashed line indicates the coastline. The open square shows Area 2.

cloud convective activity in those two zones (Fig. 9b). The Icmax anomaly was larger than 6 K over the TP (90–100°E) on the day of $t = -2$, and the soil moisture was 0.02 (cm^3 cm^{-3}) greater than that of the climatology (Fig. 9c). Around the LMCS formation day (from $t = -1$ to $t = 0$), the primary area of the ZACC shifted from the TP (about 90–105°E) to central-east China (about 100–123°E). In the upper troposphere, the geopotential height anomaly became the largest from $t = 0$ to $t = +1$, and reached 60 gpm at 102–110°E. This positive anomaly zone in geopotential height expanded to the east until $t = +3$, corresponding to the cloud convective activity. On the other hand, the distribution of larger soil moisture propagated eastward from $t = -1$ to $t = +2$. The wet land surface conditions continued to $t = +5$ in the area east of 112°E. Namely, cloud convective activity in the ZACC induced more eastward expansion of UH and obviously moistened the land surface from the TP to east China.

Focusing on the $q\mathbf{V}$ anomaly at 700 hPa (Fig. 9b, vector), the southwesterly or westerly monsoon flow prevailed to the east of 100°E a few days before LMCS generation. The magnitude of $q\mathbf{V}$ anomaly in the lower troposphere (length of vector, shaded in Fig. 9b) significantly increased after LMCS occurrence, and its maximum exceeded more than 0.04 (m s^{-1})(kg kg^{-1}) on the day at $t = +2$. This enhanced intrusion of moist southwesterly/westerly into the east of 110°E of the ZACC is also horizontally shown in Fig. 8c. Particularly, the maximum of the positive anomaly of Icmax was formed at around 112°E and 120°E at $t = +1$ (Fig. 8c), although the occurrence number of LMCS at central and east China on $t = +1$ was similar to that on $t = 0$ (Fig. 8d). According to the numerical simulation of Wang (1987), the development of a warm vortex over the TP is explained by the enhancement of the low-level convergence associated with the Conditional Instability of the Second Kind (CISK) which was caused by the latent heat release from cloud convection, complex terrain, and convergence between southerlies and northerlies at the center of the TP. On the other hand, Yasunari and Miwa (2006) identified through case studies that the

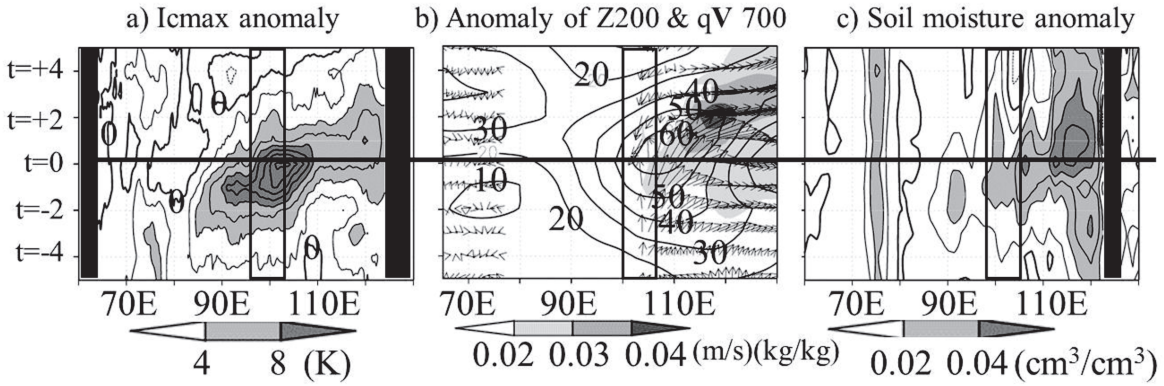

Fig. 9. Time evolution (from $t = -5$ to $t = +5$) of composite anomaly averaged between 30–35°N of a) Icmax (contour interval is 2 K), b) geopotential height at 200 hPa (gpm, contour), $q\mathbf{V}$ at 700 hPa (m s^{-1} × kg kg^{-1}; vector), and magnitude of $q\mathbf{V}$ (m s^{-1} × kg kg^{-1}; shaded), and c) soil moisture (contour interval is 0.01 cm^3 cm^{-3}) for the LMCS case of Area 2. A horizontal thick line means $t = 0$, and an open square indicates the longitude of Area 2. The black shaded area in Figure a and c is an area from which no data was obtained.

eastward movement of the vortices with cloud convective systems, which is induced in the large-scale convergence over the TP, is embedded in the Meiyu/Baiu front and triggers flooding in the middle and lower reaches of the Yangtze River. The LMCS development around the eastern part of the TP was suggested to contribute to the activation of successive precipitation systems over central-east China via the enhancement of low-level convergence of $q\mathbf{V}$ by the CISK and/or the LMCS propagation in the ZACC, as shown in those previous studies.

7. Summary and discussion

The contribution of large MCS (LMCS) formation on the eastward extension of the upper tropospheric high (UH) was investigated in the Asian monsoon region. We also verified the fluctuation of UH and land surface conditions in conjunction with the precipitation systems over China formed after LMCS generation around the eastern TP. The UH eastward expansion on a time scale of a few days was strongly linked with the LMCS formation around the eastern part of TP and a zone of active cloud convection (ZACC) over central-east China during summer. The major results are summarized as follows;

1) The area in which mature MCS appeared was examined around the TP region. The mature MCSs were extracted in six concentrated areas; the southern TP (Area 1), the eastern TP (Area 2), around the Patkai Mountains (Area 3), the southern foot of the Himalayas (Area 4), the Bay of Bengal (Area 5), and the northern part of Vietnam (Area 6). MCSs that developed in Areas 2, 5, and 6 tended to become large. In Area 2, an inland and high elevation area with little water vapor, large MCSs (larger than 1.0×10^5 km^2) accounted for 25% of all MCSs, and the diurnal variation of initiation/development of MCS was the most active. Approximately 50% of all MCSs over the Bay of Bengal (Area 5) were large, with the highest number in the Asian monsoon region. There was approximately one MCS daily in Area 6, and about 30% of them became large.

2) Fluctuation in the upper synoptic condition was revealed around the formation day of LMCS by the composite analysis using JRA25/JCDAS for Areas 2, 5, and 6. The temperature increased over 0.45 K with about 10-gpm increase of the upper geopotential height corresponding to the LMCS formation in Area 2. This UH evolution was not identified on the days of small MCS formation and the days of no MCS occurrence with high daily-averaged Ic. On the other hand, the upper geopotential height varied little from day to day for the LMCS cases of Areas 5 and 6, and the range of temperature increase in the middle and upper troposphere was also small relative to those in the LMCS cases in Area 2. From this evidence, it was concluded that the LMCS that formed in the eastern part of TP was especially important for the eastward extension of the UH.

3) On the day of LMCS development, a ZACC appeared between 30°N and 35°N from the eastern TP to

east China. Cyclonic circulation, which was enhanced in the lower troposphere of Area 2, caused northward intrusion of moist air masses and meandering of the ZACC on the northeastern side of the Sichuan Basin. Water vapor transport to the ZACC gradually strengthened, and the ZACC remained in central-east China for a few days after LMCS formation. In response to this maintenance of active cloud convection, the moistening area of land surface propagated from the TP to east China and the UH expanded farther eastward. These results also identified successive cloud convective activity in the ZACC as an additional important factor for the UH extension to the east China.

One to three days after LMCS formation, the positive anomaly of Icmax remained over the central and eastern TP (90–103°E, Fig. 9a). In the eastern part (97–103°E), the soil moisture anomaly was more than 0.02 ($cm^3\ cm^{-3}$) until $t = +4$ following the active cloud convections (Fig. 9c). It is well known that the wetness of the land surface controls the structure of cumulus cloud convections in the semi-arid regions of the world. For example, a numerical simulation by Peilke et al. (1997) indicated that a change of the land surface conditions from crop land to homogeneous grass land inhibits the formation of thunderstorms over the Great Plains in the United States via a decrease of transpiration from the vegetation and weakening of convective instability. According to precipitation observations in the Sahel by Taylor and Lebel (1998), precipitation cells in the MCS become partly activated because of inhomogeneous wet patches caused by mesoscale cloud convection a few days before the passage of MCS. From the case studies using numerical simulations in the Sahel, triggering of cloud convection is favored by drier surface and/or soil moisture inhomogeneities, while a mature cloud system weakens in the vicinity of a drier surface (Gantner and Kalthoff 2009). Land surface moistening and activation of vegetation associated with the seasonal transition of plateau monsoon change convective cloud structure and increase precipitation on the ground in the Naqu Basin over the TP (Yamada and Uyeda 2006; Yamada 2008). Our study suggests that the moist condition of the land surface due to LMCS precipitation could encourage continuing cloud convective activities over the eastern TP.

In this study, activation of $q\mathbf{V}$ intrusion and cloud convections in the ZACC were confirmed within a few days of the LMCS development. However, it was not clear whether the LMCS generated in Area 2 was moving to east or new clouds were formed in the ZACC because of active water vapor intrusion. Non-hydrostatic numerical simulations will give insight into this issue. The numerical models have dependence on the initial and boundary conditions, and considerable computational resources are needed for the increase of the simulation sample. On the other hand, the numerical model can explicitly solve the formation of cloud convection with a horizontal scale of a few km–several hundred m and can be used for sensitivity experiments, e.g., eliminating diabatic heating from clouds. The time variation of cloud convective activity in the ZACC for several consecutive days should be verified using a non-hydrostatic numerical model.

Acknowledgements

The work described in this publication has been supported by the European Commission (Call FP7-ENV-2007-1 Grant 212921) as part of the CEOP-AEGIS project (http://www.ceopaegis.org/) coordinated by the University of Strasbourg. The Meteosat5/7-IR image was provided by European Organization for the Exploitation of Meteorological Satellites (EUMETSAT). The AMSR-E soil moisture data were provided by Dr. Hideyuki Fujii at Japan Aerospace Exploration Agency (JAXA). JRA25/JCDAS was provided from the cooperative research project by the Japan Meteorological Agency (JMA) and the Central Research Institute of Electric Power Industry (CRIEPI).

References

Barros, A. P., G. Kim, E. Williams, and W. Nesbitt, 2004: Probing orographic controls in the Himalayas during the monsoon using satellite imagery. *Natural Hazards and Earth System Sciences*, **4**, 29–51.

Camago, S. J., A. W. Robertson, S. J. Gaffney, P. Smyth, and M. Ghil, 2007: Cluster analysis of typhoon tracks. Part 1: General properties. *J. Climate*, **20**, 3635–3653.

Chen, S., and R. A. Houze, 1997: Diurnal variation and lifecycle of deep convective systems over the tropical Pacific warm pool. *Quart. J. Roy. Meteor. Soc.*, **123**, 357–388.

Enomoto, T., B. J. Hoskins, and Y. Matsukda, 2003: The formation mechanism of the Bonin high in August. *Quart. J. Roy. Meteor. Soc.*, **129**, 157–178.

Evans, L. J., and R. E. Shemo, 1996: A procedure for automated satellite-based identification and climatology development of various classes of organized convection. *J. Appl. Meteor.*, **35**, 638–652.

Fujii, H., T. Koike, and K. Imaoka, 2009: Improvement of the AMSR-E algorithm for soil moisture estimation by introducing a fractional vegetation converage dataset derived from MODIS data. *Journal of The Remote Sensing Society of Japan*, **29**, 282–292.

Fujinami, H., and T. Yasunari, 2001: The seasonal and in-

traseasonal variability of diurnal cloud activity over the Tibetan Plateau. *J. Meteor. Soc. Japan*, **79**, 1207–1227.

Fujinami, H., and T. Yasunari, 2004: Submonthly variability of convection and circulation over and around the Tibetan Plateau during the boreal summer. *J. Meteor. Soc. Japan*, **82**, 1545–1564.

Fujinami, H., and T. Yasunari, 2009: The effects of midlatitude waves over and around the Tibetan Plateau on submonthly variability of the East Asian summer monsoon. *Mon. Wea. Rev.*, **126**, 1597–1607.

Gantner, L., and N. Kalthoff, 2009: Sensitivity of a modeled life cycle of a mesoscale convective system to soil conditions over West Africa. *Quart. J. Roy. Meteor. Soc.*, **135**, doi:10.1002/qj.425.

He, H., J. McGinnis, Z. Song, and M. Yanai, 1987: Onset of the Asian summer monsoon in 1979 and the effect of the Tibetan Plateau. *Mon. Wea. Rev.*, **115**, 1966–1996.

Houze, J. R., C. Darren, and B. F. Smull, 2007: Monsoon convection in the Himalayan region as seen by the TRMM precipitation radar. *Quart. J. Roy. Meteor. Soc.*, **133**, doi:10.1002/qj.106.

Hsu, H.-H., C.-T. Terng, and C.-T. Chen, 1999: Evolution of large-scale circulation and heating during the first transition of Asian summer monsoon. *J. Climate*, **12**, 793–810.

Islam, Md. N., T. Hayashi, H. Uyeda, T. Terao, and K. Kikuchi, 2004: Diurnal variations of cloud activity in Bangladesh and north of the Bay of Bengal in 2000. *Remote Sens. Environ.*, **90**, 378–388.

Koike, T., Y. Nakamura, I. Kaihotsu, G. Davva, N. Matsuura, K. Tamagawa, and H. Fujii, 2004: Development of an Advanced Microwave Scannig Radiometer (AMSR-E) algorithm of soil moisture and vegetation water content. *Annual Journal of Hydraulic Engineering*, **48**, 217–222, (In Japanese with English abstract).

Krishnamurti, T. N., S. M. Daggupaty, J. Fain, M. Kanamitsu, and J. D. Lee, 1973: Tibetan High and upper tropospheric tropical circulations during northern summer. *Bull. Amer. Meteor. Soc.*, **54**, 1234–1249.

Laing, A. G., and J. M. Fritsch, 1993: Mesoscale convective complexes over the Indian monsoon region. *J. Climate*, **6**, 911–919.

Li, C., and M. Yanai, 1996: The onset and interannual variability of the Asian summer monsoon in relation to land-sea thermal contrast. *J. Climatol.*, **9**, 358–375.

Li, Y., W. Yun, S. Yang, H. Liang, G. Shouting, and R. Fu, 2008: Characteristics of summer convective systems initiated over the Tibetan Plateau. Part 1: Origin, track, development, and precipitation. *J. Appl. Meteor. Climatol.*, **47**, 2679– 2695.

Mao, J., and G. Wu, 2006: Intraseasonal variation of the Yangtze rainfall and its related atmospheric circulation features during the 1991 summer. *Climate Dyn.*, **27**, 815–830.

Murakarami, M., 1983: Analysis of the deep convective activity over the western pacific and southeast Asia. *J. Meteor. Soc. Japan*, **61**, 60–76.

Nitta, T., 1983: Observational study of heat sources over the eastern Tibetan Plateau during the summer monsoon. *J. Meteor. Soc. Japan*, **61**, 590–604.

Ohsawa, T., H. Ueda, T. Hayashi, A. Watanabe, and J. Matsumoto, 2001: Diurnal variations of convective activity and rainfall in Tropical Asia. *J. Meteor. Soc. Japan*, **79**, 333–352.

Onogi, K., J. Tsutsui, H. Koide, M. Sakamoto, S. Kobayashi, H. Hatsushika, T. Matsumoto, N. Yamazaki, H. Kamahori, K. Takahashi, S. Kadokura, K. Wada, K. Kato, R. Oyama, T. Ose, N. Mannoji, and R. Taira, 2007: The JRA-25 Reanalysis. *J. Meteor. Soc. Japan*, **85**, 369–432.

Peilke, A. R., T. J. Lee, J. H. Copeland, J. L. Eastman, C. L. Ziegler, and C. A. Finley, 1997: Use of USGS-provided data to improve weather and climate simulations. *Ecol. Appl.*, **7**, 3–21.

Sugimoto, S., and K. Ueno, 2010: Formation of mesoscale convective systems over the eastern Tibetan Plateau affected by plateau-scale heating contrasts. *J. Geophys. Res.*, **115**, D16105, doi:10.1029/2009JD013609.

Tamura, T., K. Taniguchi, and T. Koike, 2010: Mechanism of upper tropospheric warming around the Tibetan Plateau at the onset phase of the Asian summer monsoon. *J. Geophys. Res.*, **115**, D02106, doi:10.1029/2008JD011678.

Tao, S., and Y. Ding, 1981: Observational evidence of the influence of the Qinghai-Xizang (Tibet) Plateau on the occurrence of heavy rain and severe convective storms in China. *Bull. Amer. Meteor. Soc.*, **62**, 23–30.

Taylor, M. C., and T. Lebel, 1998: Observation evidence of persistent convective-scale rainfall patterns. *Mon. Wea. Rev.*, **126**, 1597–1607.

Terao, T.,1998: Barotropic disturbances on intraseasonal time scales observed in the midlatitudes over the Eurasian continent during the northern summer. *J. Meteor. Soc. Japan*, **76**, 419–436.

Ueda, H., and T. Yasunari, 1998: Role of warming over the Tibetan Plateau in early onset of the summer monsoon over the Bay of Bengal and the South China Sea. *J. Meteor. Soc. Japan*, **76**, 1–12.

Ueno, K., S. Sugimoto, T. Koike, H. Tsutsui, and X. Xu, 2011: Generation processes of mesoscale convective systems following midlatitude troughs around the Sichuan Basin. *J. Geophys. Res.*, **116**, D02104, doi:10.1029/2009JD013780.

Uyeda, H., H. Yamada, J. Horikomi, R. Shirooka, S. Shimizu, L. Liuping, K. Ueno, H. Fujii, and T. Koike, 2001: Characteristics of convective clouds observed by a Doppler radar at Naqu on Tibetan Plateau during the GAME-Tibet IOP. *J. Meteor. Soc. Japan*, **79**, 463–474.

Wang, B., 1987: The development mechanism for Tibetan Plateau warm vortices. *J. Atmos. Sci.*, **44**, 2978–2994.

Xie, L., and K. Ueno, 2011: Differences of synoptic fields depending on the location of MCS genesis in southwest China. *Tsukuba Geoenvironmental Sciences*, **7**, 3–11.

Yamada, H., and H. Uyeda, 2006: Transition of the rainfall characteristics related to the zmoistening of the land surface over the central Tibetan Plateau during the summer of 1998. *Mon. Wea. Rev.*, **134**, 3230–3247.

Yamada, H., 2008: Numerical simulations of the role of land surface conditions in the evolution and structure of summertime thunderstorms over a flat highland. *Mon. Wea. Rev.*, **136**, 173–188.

Yanai, M., C. Li, and Z. Song, 1992: Seasonal heating of the Tibetan Plateau and its effects on the evolution of the Asian summer monsoon. *J. Meteor. Soc. Japan*, **70**, 319–351.

Yang, G.-Y., and J. Slingo, 2001: The Diurnal cycle in the Tropics. *Mon. Wea. Rev.*, **129**, 784–801.

Yasunari, T., and T. Miwa, 2006: Convective cloud systems ovr the Tibetan Plateau and their impact on meso-scale disturbances in the Meiyu/Baiu Frontal zone. *J. Meteor. Soc. Japan*, **84**, 783–803.

Yatagai, A., and T. Yasunari, 1995: Interannual variations of summer precipitation in the arid/semi-arid regions in China and Mongolia: Their regionality and relation to the Asian summer monsoon. *J. Meteor. Soc. Japan*, **73**, 909–923.

Yu, R., T. Zhou, A. Xiong, Y. Zhu, and J. Li, 2007: Diurnal variations of summer precipitation over contiguous China. *Geophys. Res. Lett.*, **34**, L01704, doi:10.1029/2006GL028129.

Zhang, Q., G. Wu, and Y. Qian, 2002: The bimodality of the 100 hPa South Asia High and its relationship to climate anomaly over East Asia in summer. *J. Meteor. Soc. Japan*, **80**, 733–744.

Zhou, T., and R. Yu, 2005: Atmospheric water vapor transport associated with typical anomalous summer rainfall patterns in China. *J. Geophys. Res.*, **110**, D08104, doi:10.1029/2004JD005413.

Zhou, T., R. Yu, H. Chen, A. Dai, and Y. Pan, 2008: Summer precipitation frequency, intensity, and diurnal cycle over China: A comparison of satellite data with rain gauge observations. *J. Climate*, **21**, 3997–4010.

Zhou, T., R. Yu, J. Zhang, H. Drange, C. Cassou, C. Deser, D. L. R. Hodson, E. Sanchez-gomez, J. Li, N. Yside, X. Xin, and Y. Okumura, 2009: Why the western pacific subtropical high has extended westward since the late 1970s. *J. Climate*, **22**, 2199–2215.

Zuidema, P., 2003: Convective clouds over the Bay of Bengal. *Mon. Wea. Rev.*, **131**, 780–798.